Astronomy
&
Astrophysics

Comparative chemistry of diffuse clouds. IV: CH

H. Liszt[1] and R. Lucas[2]

[1] National Radio Astronomy Observatory, 520 Edgemont Road, Charlottesville, VA 22903-2475, USA
[2] Institut de Radioastronomie Millimétrique, 300 Rue de la Piscine, 38406 Saint Martin d'Hères, France

Abstract. We observed the 3335 MHz (λ 9 cm) $F = 1$–1 line of CH toward a sample of diffuse clouds occulting compact extragalactic mm-wave continuum sources, using the old NRAO 43m telescope. Because radiofrequency observations of CH really must be calibrated with reference to a known CH abundance, we begin by deriving the relationships between CH, E_{B-V}, H_2 and other hydrides found by optical spectroscopy. No simple relationship exists between N(CH) and E_{B-V}, since N(CH) is strongly bimodal with respect to reddening for $E_{B-V} < 0.3$ mag and the typical range in the N(CH)/E_{B-V} ratio is an order of magnitude or more at any given $E_{B-V} > 0.3$ mag. However, N(CH)/N(H$_2$) = $4.3 \pm 1.9 \times 10^{-8}$ in the mean and N(CH) $\propto N$(H$_2$)$^{1.00 \pm 0.06}$ for $10^{19} < N$(H$_2$) $< 10^{21}$ cm^{-2}. If CH is a good predictor of H$_2$, 40%–45% of the hydrogen in the local diffuse/translucent ISM is in the molecular form at the accepted mean density, higher than previous estimates found in samples of lower-than-average mean density. Optical observations of the population ratios in the upper and lower halves of the CH lambda-doublet suggest that the brightness of the 3335 MHz CH line should be double-valued at a given CH column density in diffuse gas: double-valuedness is noticeable in our data when comparing CH with CO or HCO$^+$. The CH brightness at 3335 MHz is mildly bimodal with respect to CO emission in our diffuse cloud data but much more strongly bimodal when comparing diffuse or translucent gas and dark gas. The CH Λ-doublet is generally inverted in diffuse gas but we did not succeed in measuring the excitation temperature except toward 3C123 where we confirm one older value $T_{\rm exc} \approx -10$ K.

Key words. ISM: molecules

1. Introduction

Some chemical species present in diffuse interstellar gas can only be studied in optical/uv absorption: these include C$_2$ (Chaffee & Lutz 1978), NH (Meyer & Roth 1991; Crawford & Williams 1997), HCl (Federman et al. 1995), and most importantly H$_2$ (Savage et al. 1977). Many more, chiefly polyatomics and heavy diatomics, are seen only in the radio regime. These include H$_2$CO (Federman & Willson 1982; Liszt & Lucas 1995), C$_3$H$_2$ (Cox et al. 1988; Lucas & Liszt 2000a), NH$_3$ (Nash 1990), HCO$^+$ (Liszt & Lucas 1996, 2000), C$_2$H (Lucas & Liszt 2000a), HCN and HNC (Liszt & Lucas 2001), SiO (Lucas & Liszt 2000b), and sulfur-bearing species such as CS, SO, H$_2$S, HCS$^+$ etc. (Lucas & Liszt 2002).

The few species which overlap both domains (CH, OH, CN and CO) provide an important bridge between two rather different ways of studying interstellar chemistry in diffuse clouds. CN, for instance, whose relationships with CH, C$_2$, CO and H$_2$ are well-studied optically (Federman et al. 1994; van Dishoeck & Black 1989; Federman & Lambert 1988), is closely tied to HCN and HNC and more loosely related to perhaps a dozen other polyatomic species seen at mm-wavelengths (Liszt & Lucas 2001). Similarly OH, whose abundance relative to H$_2$ was found by Crutcher (1979) to be constant over a wide range of extinction, is closely tied to HCO$^+$ (Liszt & Lucas 1996;

Lucas & Liszt 1996; Liszt & Lucas 2000), leading us to believe that the relative abundance of HCO$^+$ also varies little. HCO$^+$ is the immediate progenitor of CO in diffuse gas (Glassgold & Langer 1975, 1976; Van Dishoeck & Black 1986). Its unexpectedly large abundance relative to H$_2$ is sufficient to explain the run of N(CO) with N(H$_2$) for $2 \times 10^{19} < N$(H$_2$) $< 2 \times 10^{21}$ cm^{-2}. $4 \times 10^{12} < N$(CO) $< 2 \times 10^{16}$ cm^{-2} (Liszt & Lucas 2000).

CH, the subject of this study, represents another important bridge between the optical and radio regimes, all the more so because its abundance relative to molecular hydrogen is very well-determined and nearly fixed for lines of sight having $A_V \leq 3$ (Federman & Lambert 1988; Danks et al. 1984; Federman 1982). A determination of its column density in the gas toward our compact extragalactic mm-wave continuum background sources would provide an important check on the abundances of all the other species we detect. Unfortunately, observation of CH at 3335 MHz in the radio regime is presently impossible and opportunities will be at best severely restricted in the future. Of the large single dishes, only Arecibo and Nançay apparently have current plans to provide a receiver in the 9 cm waveband. Eventually, the complete frequency coverage of the EVLA will make possible widespread study of CH in stimulated emission against continuum sources, although the usefulness of such work, absent complementary emission studies, may be somewhat limited.
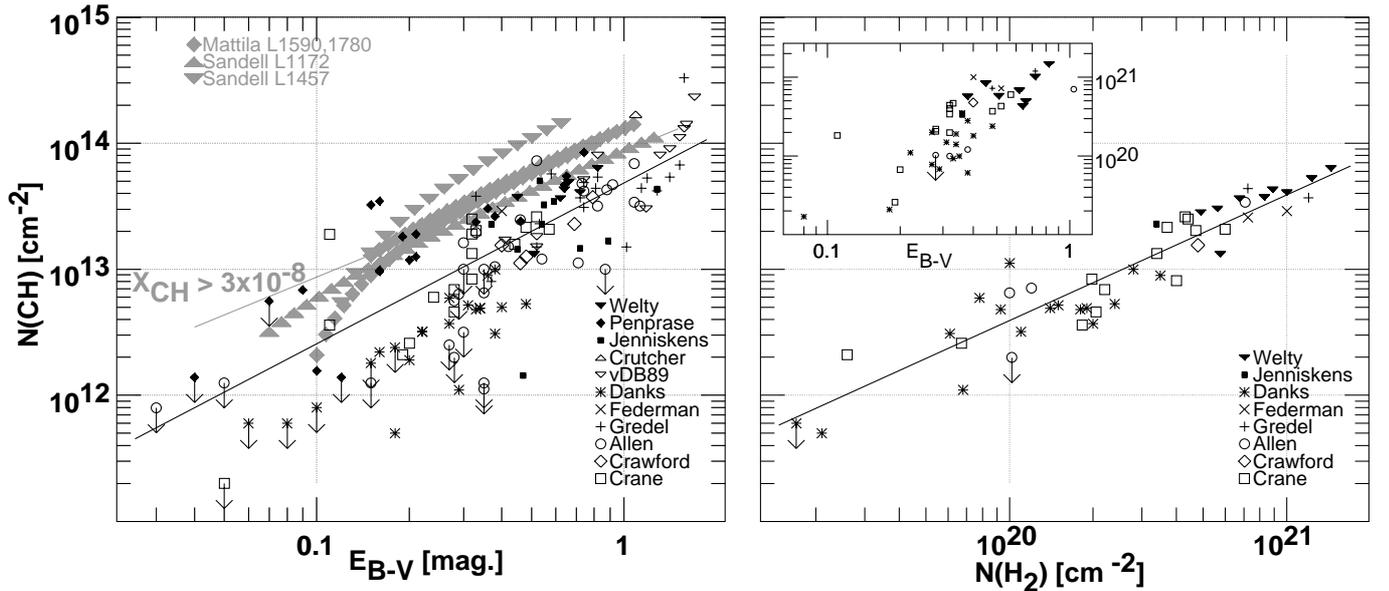
Fig. 1. The dependence of optically-measured CH column densities on reddening (left panel) and $N(H_2)$. CH Data are from Crane et al. (1995), Crawford (1995), Allen (1994), Gredel et al. (1993), Federman et al. (1994), Danks et al. (1984), van Dishoeck & Black (1989), Crutcher (1985), Jenniskens et al. (1992), Penprase (1993) and Welty et al. as tabulated in Rachford et al. (2002).
The H_2 column densities are from Savage et al. (1977) and Rachford et al. (2002) except for one line of sight each from Joseph et al. (1986), Snow et al. (2000) and Rachford et al. (2001). Superposed in the left panel are the $N(CH)-E_{B-V}$ loci derived from the dark cloud studies of Mattila (1986) for L1590 and L1780, and Sandell (1982) for L1172 and L1457; also shown there is the line corresponding to $X_{CH} \approx 2N(CH)/N(H) = 3 \times 10^{-8}$ as discussed in the text. Superposed in the right-hand panel are a plot of $N(H_2)$ vs. E_{B-V} for sightlines with measured $N(CH)$ and the best-fit power-law regression line (see Sect. 2.2).

In this work we present 3335 MHz $F = 1-1$ CH observations in the direction of compact extragalactic continuum sources which we have previously observed in an extensive, ongoing study of mm-wave absorption line chemistry. We took data toward and around these and two other sources which have stronger cm-wave continuum and are occulted by denser (but not necessarily darker) gas (i.e. 3C123 and 3C133), in much the same way as we did earlier for OH (Liszt & Lucas 1996; Lucas & Liszt 1996) and H_2CO (Liszt & Lucas 1995). We did so at least partly for the purpose of deriving the excitation temperature in diffuse gas and did not see any true CH absorption: the optical depth was either negative, owing to the well-known collisionally-induced inversion of the ground-state lambda-doublet (Bertojo et al. 1976; Bujarrabal et al. 1984; Bouloy et al. 1984), or immeasurably small. The CH transition is almost certainly inverted in the diffuse gas we observed but excitation studies will require a telescope gain much larger and a telescope beam much smaller than that afforded by the old NRAO 43 m antenna. In the absence of much direct evidence allowing a calibration of the relationship between $N(CH)$ and the microwave brightness in diffuse gas, we resort to a discussion of the rich body of optical CH measurements in the diffuse ISM.

The plan of the present paper is as follows. In Sect. 2 we derive the abundance of CH with respect to E_{B-V}, H_2 and other hydrides, using optical absorption line observations, and we note the implications of optical studies of the excitation of the ground-state CH Λ-doublet for microwave observations. In Sect. 3 we describe our new 9 cm observations of the 3335 MHz CH $F = 1-1$ (main) line, and compare them

to our prior results for OH, HCO^+, C_2H and CO in the same directions. Section 4 is a brief summary.

2. Optical absorption line studies of CH

2.1. The relationship between CH and E_{B-V}

Much of the original rationale for using CH as a tracer of H_2 was the relationship $N(CH) = 6.3 \times 10^{13}$ cm^{-2} E_{B-V} derived by Lang & Willson (1978) using a combination of optical and microwave determinations of $N(CH)$ along some twenty lines of sight; for instance, see Mattila (1986) which forms the basis of the discussion by Magnani & Onello (1995). The microwave determinations are subject to considerable uncertainty (at least comparatively) so that an optical determination of $N(CH)$ is preferable, at least initially. Lien (1984) shows how to derive $N(CH)$ properly from the available CH optical absorption lines.

Figure 1 at left shows the run of $N(CH)$ with E_{B-V} found in a much larger sample of more recent optical measurements (Allen 1994; Crane et al. 1995; Crawford 1995; Federman et al. 1994; Gredel et al. 1993; Danks et al. 1984; van Dishoeck & Black 1989; Crutcher 1985; Jenniskens et al. 1992; Penprase 1993) including the data of Welty et al. tabulated in Rachford et al. (2002). Represented are 140 lines of sight harboring 120 CH detections: many uninformative upper limits contained in the original references were not transcribed. The most recent measurement was used in those cases where lines of sight had been observed more than once. It is not possible to infer a single (or single-valued) or linear relationship between $N(CH)$ and E_{B-V}.
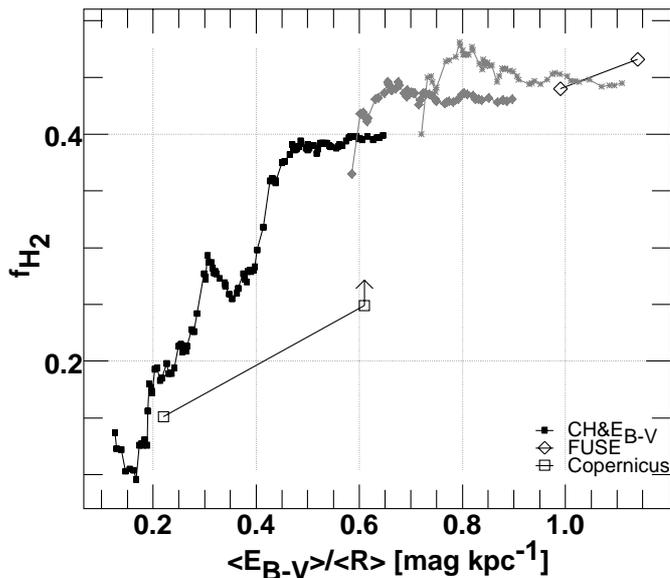
Fig. 2. The fraction of H-nuclei in H_2 derived by various means. The connected symbols labeled "Copernicus" represent the results of Bohlin et al. (1978), measured (at left) and corrected for bias to lower than average mean density. The chained curves represent samples of the sightlines with measured $N(CH)$, assuming the same $N(H)-E_{B-V}$ conversion and $X_{CH} = 4.3 \times 10^{-8}$ as described in Sect. 2.2.1

For $E_{B-V} < 0.3$, $N(CH)$ is largely bimodal, i.e. either $N(CH) \lesssim 3 \times 10^{12}$ cm^{-2}, in, presumably, typical diffuse gas, or $N(CH) > 10^{13}$ cm^{-2} in the CO-emission-selected, high-latitude objects studied by Penprase (1993) and along one of the sightlines studied by Crane et al. (1995). In these directions, the gas is apparently dense enough or sufficiently poorly-illuminated for the great majority of hydrogen to have been converted into H_2 even for $A_V < 1$. The transition to consistently high CH abundances occurs somewhere in the range $0.1 \leq E_{B-V} \leq 0.4$; many lines of sight with $E_{B-V} = 0.3$ mag do not show CH and one at $E_{B-V} = 0.87$ from Allen (1994) is underabundant compared to the mean by about a factor of 3.

Many of the points seem to lie along a band increasing approximately as $N(CH) \propto E_{B-V}^{1.8}$ for $0.1 \leq E_{B-V} \leq 1$; this arises because $N(H_2)$ increases with E_{B-V} and $X_{CH} \equiv N(CH)/N(H_2)$ is approximately constant (see Sect. 2.2). The enormous variance of the observed $N(CH)$ values near $E_{B-V} = 0.3$ mag seems quite extraordinary even if order-of-magnitude variations in $N(CH)$ are common at most other E_{B-V} as well. Perhaps a second transition to yet more fully molecular gas will become evident in the $N(H_2)-E_{B-V}$ relationship as more data become available.

Shown in the left-hand panel of Fig. 1 is the line $N(CH) = 3 \times 10^{-8} \times 5.8 \times 10^{21} E_{B-V}$ cm$^{-2}/2$, the maximum CH column density which could arise if $X_{CH} = 3 \times 10^{-8}$ and all gas along the line of sight were in the form of H_2 (i.e. E_{B-V} is converted to a column density of H-nuclei using the standard value of Bohlin et al. 1978). Apparently, a few sightlines with reddening as small as 0.1–0.2 mag have X_{CH} approaching 10^{-7}.

Superposed in the left panel of Fig. 1 we have included the mean CH$-A_B$ loci derived for several dark clouds from microwave measurements of the 3335 MHz line, using

$A_B = 4E_{B-V}$ as in the original references. In what follows we will denote by $N_\mu(CH)$ a CH column density derived by converting a microwave CH intensity using standard formulae. For comparison, then, we note that Mattila (1986) used the 3335 MHz line of CH to derive $N_\mu(CH) = (13.9 \pm 1.2) \times 10^{13}$ cm^{-2} ($E_{B-V} - 0.085$) and $N_\mu(CH) = (13.9 \pm 1.2) \times 10^{13}$ cm^{-2} ($E_{B-V} - 0.06$) in the two dark clouds L1590 and L1780. Sandell (1982) found relationships $N_\mu(CH) = 27.2 \times 10^{13}$ cm^{-2} ($E_{B-V} - 0.1$) for L1457 and $N_\mu(CH) = 9.2 \times 10^{13}$ cm^{-2} ($E_{B-V} - 0.03$) for L1172 while the much more limited data for L1642 in Table 4 of Sandell et al. (1981) have a limiting slope of $N_\mu(CH)/E_{B-V} = 11.2 \times 10^{13}$ cm^{-2}.

There is a very substantial range in the limiting behaviour of the derived $N_\mu(CH)/E_{B-V}$ ratios in these objects, and all are much higher than orignally derived in the work of Lang & Willson (1978). Nonetheless, they do in general correspond fairly well to the values of X_{CH} seen in the upper reaches of the CH column densities derived optically. The use of high $N(CH)/E_{B-V}$ ratios is probably acceptable, even at low E_{B-V}, for CO-emitting gas.

2.2. The relationship between CH and H_2

Much of the behaviour seen in the left-hand panel of Fig. 1 can be understood simply on the basis of the observed variation of $N(H_2)$ with reddening, and a fixed or nearly-fixed abundance of CH relative to H_2. Such a nearly linear relationship between $N(CH)$ and $N(H_2)$ was demonstrated by Federman (1982) and by Danks et al. (1984) and relatively little had changed in the intervening time vis-a-vis H_2 until the recent FUSE survey work of Rachford et al. (2002). The CH profiles have improved somewhat in quality and number and the important reanalysis by Lien (1984) clarified the interpretation greatly. Figure 1 at right shows the current situation, from which, for the lines of sight with detections of both CH and H_2, we derive $\log N(CH) = (-7.35 \pm 1.31) + (1.00 \pm 0.06) \log N(H_2)$. A less comprehensive version of this diagram which provided very nearly the same regression line was shown by Magnani et al. (1998).

In the mean, $X_{CH} = 4.3 \pm 1.9 \times 10^{-8}$. The ±45% variance of $N(CH)$ about $N(H_2)$ is appreciable; it sets the ultimate limit on expectations of the reliability of CH as a predictor of H_2. These data represent sightline averages over multiple components and do not prove that the CH abundance is constant in individual clouds of higher density and extinction. Indeed, the dark cloud data discussed in Sect. 2.4 show that X_{CH} declines markedly in darker gas and a steady decline from diffuse to dark conditions has been noted since the original microwave surveys of Rydbeck et al. (1976), Hjalmarson et al. (1977) and Mattila (1986). The diminished scatter in Fig. 2 at right for the lines of sight having the highest $N(H_2)$ is strongly suggestive of blending.

As shown in the inset in the right-hand panel of Fig. 1, much of the scatter in the plot of $N(CH)$ vs. E_{B-V} can be understood simply in terms of the variation of $N(H_2)$ with E_{B-V}, given that X_{CH} is approximately constant. Along lines of sight where H_2 is known directly, $N(H_2)$ increases approximately as

Table 1. Column densities of hydrides in diffuse and dark gas.

	ζ Oph	ζ Per	o Per	HD27778	TMC-1[5]	L134N[5]
	$N(\text{cm}^{-2})$	$N(\text{cm}^{-2})$	$N(\text{cm}^{-2})$	$N(\text{cm}^{-2})$	$N_\mu(\text{cm}^{-2})$	$N_\mu(\text{cm}^{-2})$
CH[1]	2.50E13	2.03E13	1.90E13	2.90E13	2E14	1E14
NH[2]	8.8(1.2)E11	9.0(0.2)E11		2.7(0.6)E12		
OH[3]	4.7(0.7)E13	4.1(0.4)E13	7.8 (2.6)E13	10.2(0.4)E13	3E15	7.5E14
H$_2$[4]	4.4E20	4.8E20	4.0E20	1.0(0.3)E21	(1E22)	(1E22)

[1] $N(\text{CH})$ from Crane et al. (1995) except HD27778 from Federman et al. (1994).

[2] $N(\text{NH})$ from Meyer & Roth (1991) except ζ Oph from Crawford & Williams (1997).

[3] $N(\text{OH})$ from Roueff (1996) and Felenbok & Roueff (1996).

[4] $N(\text{H}_2)$ from Savage et al. (1977) except HD27778 from Joseph et al. (1986).

[5] Dark-cloud data from Ohishi et al. (1992).

$E_{B-V}^{1.8}$ for $E_{B-V} > 0.2$. The Penprase (1993) sample, selected on the basis of relatively strong CO $J = 1–0$ emission, probably represents a special circumstance whereby the molecular fraction is high even below $E_{B-V} = 0.3$.

2.2.1. The fraction of gas in molecular form

The fraction of gas in molecular form in the local ISM is an important quantity which provides interesting constraints on interpretations of atomic and molecular gas constituents independently. Here we take a new approach to determining a local mean for $f_{\text{H}_2} \equiv 2\,N(\text{H}_2)/(N(\text{H I}) + 2N(\text{H}_2))$, based on the near-constancy of X_{CH} and the existence of a substantial set of CH measurements which sample a wider range of mean line-of-sight densities than has been directly observable in H I and H$_2$: a sample whose mean density is more nearly equal to that of the true mean in the local ISM offers the possibility that the mean molecular gas fraction might be more representative of the overall molecular fraction in the nearby ISM as well.

Shown in Fig. 2 are the results of estimating $<f_{\text{H}_2}>$ in three ways. The symbols labelled "Copernicus" are taken from Bohlin et al. (1978) and represent their results along nearly 100 lines of sight of much lower than average mean density $<E_{B-V}>/<R> = 0.22 \text{ mag kpc}^{-1}$. The accepted mean is $0.61 \text{ mag kpc}^{-1}$, from Spitzer (1978) based on the earlier discussion of Münch (1952)[1]. The symbol at lower mean density is the actual measurement; at higher mean density it is their estimate of the true value, corrected for bias. The symbols labelled "FUSE" represent the new data of Rachford et al. (2002); the symbol at lower mean density represents only those lines of sight for which $N(\text{H I})$ was not estimated by assuming a proportionality to E_{B-V}. The chained lines labelled "CH&E_{B-V}" represent samples of the lines of sight with CH measurements, assuming $N(\text{H}_2) = N(\text{CH})/4.3 \times 10^{-8}$ and $N(\text{H}) = N(\text{H I}) + 2N(\text{H}_2) = 5.8 \times 10^{21} \text{ cm}^{-2} E_{B-V}$, so that $<N(\text{H}_2)>/<N(\text{H})> = 4.01 \times 10^{-15} <N(\text{CH})>/<E_{B-V}>$, as we now discuss.

To construct the CH-based samples, we sorted the lines of sight in order of increasing individual E_{B-V}/R and derived

$<N(\text{H}_2)>/<N(\text{H})>$ for contiguous, progressively larger samples of four or more sightlines beginning at different lower cutoffs. Where only upper limits on $N(\text{CH})$ were available, $N(\text{H}_2)$ was taken to be zero. So each chained line segment in Fig. 2 shows the mean molecular fraction, derived under the idealized assumption of a constant CH abundance and gas-dust ratio, as the sample mean extinction per unit distance varies. The dark, left-most line labelled "CH&E_{B-V}" begins at the lowest observed E_{B-V}/R and contains all lines of sight at its rightmost extent; it just barely extends beyond $<E_{B-V}>/<R> = 0.61 \text{ mag kpc}^{-1}$ when all the lines of sight are included.

The Copernicus and FUSE measurements (not the "corrected" Copernicus estimate) agree entirely with the CH-based samples; the high mean molecular fraction seen by FUSE should not be dismissed as biased because of the high sample mean density. From the CH data we see that the mean molecular fraction appears to increase fairly rapidly at low sample mean densities and is of order 0.4–0.45 at the accepted local mean density.

2.3. Population ratios

As noted in the Introduction, the excitation temperatures of the microwave CH transitions, needed to convert observed brightnesses to column density in diffuse gas, have not been (and probably cannot be) determined from microwave observations. However, Lien (1984) pointed out that the populations of the upper and lower levels of the ground-state CH Λ-doublet could be derived separately by observing different optical absorption lines (see his Fig. 2). He derived the excitation temperature T_{exc} from extant observations toward several well-studied stars and found that it could be either slightly negative or positive, but with rather large uncertainty. Extant models of CH excitation by Bertojo et al. (1976) predicted a transition from normal excitation ($T_{\text{exc}} > 0$ K) to substantial inversion ($T_{\text{exc}} = -0.6$ K) at a density somwehere between 10^2 and 10^3 H$_2$ cm^{-3}, so it was (and is) reasonable to believe that both branches of the excitation conditions would manifest themselves in diffuse gas.

Jura & Meyer (1985) rose to the challenge of taking data sufficiently accurate for this purpose and their results are summarized in Fig. 3 here. The horizontal axis is the excitation temperature of the Λ-doublet (the optical structure does not
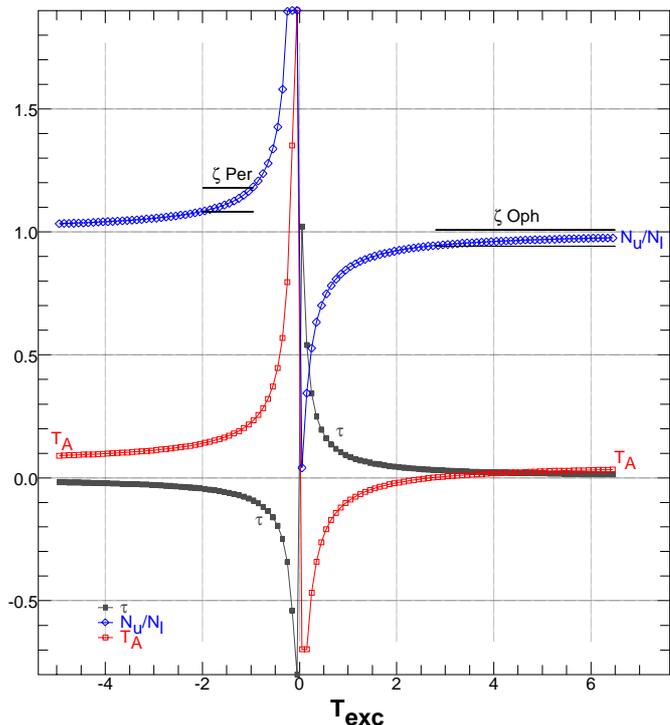
---

[1] Reddening per unit distance has units of density if $E_{B-V} \propto N(\text{H})$; R is the distance to a background star. See Spitzer (1978).

The $+1\sigma$ error bar for ζ Oph also has a branch to the far left (since it lies above unity in the population ratio) and population ratios above unity are consistent with the ζ Oph measurements at about the 1σ level.

The optically-derived population ratios nominally predict that the microwave brightness should be much larger for ζ Per; a factor three is cited by Jura & Meyer (1985), even given that N(CH) is 25% higher toward ζ Oph. However, this is not observed to be the case. Both directions have main-line profile integrals (integrated antenna temperature) of 0.08–0.09 K km s^{-1} if our results for ζ Oph (shown below and in Liszt 1997) can be compared to those of Hjalmarson et al. (1977) or Willson (1981) for ζ Per. Unfortunately, this similarity was obscured for Jura & Meyer (1985) because Lien (1984) quoted a profile integral which was twice as large for ζ Per as for ζ Oph.

It appears that the 3335 MHz CH line toward both stars is inverted, with (nominally) $T_{exc} \approx -5$ K for ζ Oph and $T_{exc} \approx -3$ K for ζ Per, if the broad microwave and narrow optical lines of sight sample approximately equal values of N(CH)[2]. These $|T_{exc}|$ are small enough that a noticeable error occurs if N_μ(CH) is derived in the limit $T_{exc} \rightarrow -\infty$; N(CH) would be overestimated by 60–100%.

In summary, even though the radio data do not show the most extreme differences in excitation suggested (but not absolutely required) by the optical results, CH in the diffuse ISM could in principle be inverted (perhaps fairly strongly) or not, and we should be prepared to encounter situations where the the same N(CH) can produce different microwave CH profile integrals and N_μ(CH). The usual practice of deriving N_μ(CH) in the limit of weak inversion is not necessarily appropriate in all diffuse gas.

2.4. Abundances of hydrides in diffuse and dark gas

Shown in Table 1 are the optically-determined column densities of the simple hydrides of C, N, and O in the only directions in which they may be compared. Taking weighted averages, we have for the means and their formal variance – taken over a very limited range of N(H$_2$) – N(CH)/N(H$_2$), $4.4 \pm 1.0 \times 10^{-8}$; N(OH)/N(H$_2$), $1.0 \pm 0.2 \times 10^{-7}$; N(NH)/N(H$_2$), $1.9 \pm 0.1 \times 10^{-9}$; N(OH)/N(CH), 3.0 ± 0.9; N(OH)/N(NH), 50.9 ± 5.1.

Also shown are the microwave-determined column densities of OH and CH toward TMC-1 and L134N, taken from Ohishi et al. (1992). X_{CH} declines markedly (a factor of 2–4) when carbon is in the form of CO rather than C$^+$, while X_{OH} remains constant or increases slightly.

3. Microwave CH lines in diffuse gas

3.1. Data and new 3335 MHz observations

The new 3335 MHz $F = 1$–1 CH observations discussed here were taken with the now-defunct NRAO 43 m antenna in 1995 September. The data taken toward ζ Oph were reported previously in Liszt (1997). The continuum background sources

---

Fig. 3. Population of the CH Λ-doublet. Plotted as a function of the excitation temperature of the CH ground-state Λ-doublet are the population ratio of the upper and lower states N_u/N_l (upper curve; chained diamonds) and the optical depth (shaded) and antenna temperature of the 3335 MHz $F = 1$–1 transition for N(CH)/$\Delta V = (N_u + N_l)/\Delta V = 2.5 \times 10^{13}$ cm^{-2} (km s^{-1})$^{-1}$, $\eta_B = 0.7$. The horizontal bars labelled "ζ Per" and "ζ Oph" represent the $\pm 1\sigma$ range of population ratios observed by Jura & Meyer (1985). See Sect. 2.3 of the text.

---

resolve the hyperfine splitting). We define T_{exc} in the usual way by asserting that the upper and lower halves of the doublet (which have equal statistical weights) are in the ratio $N_u/N_l = \exp(-h\nu/kT_{exc})$ with $\nu = 3335$ MHz, $h\nu/k = 0.160$ K corresponding to the so-called main ($F = 1$–1) line. We further assume that the excitation temperature of the doublet as a whole applies to the microwave lines individually, and plot the antenna temperature and optical depth of the $F = 1$–1 line assuming a beam efficiency of $\eta_B = 0.7$ and N(CH)/$\Delta V = (N_u + N_l)/\Delta V = 2.5 \times 10^{13}$ cm^{-2} (km s^{-1})$^{-1}$, using the column density observed toward ζ Oph (see Table 1; formulae sufficient to reproduce this plot are given in Sect. 3.1). The plotted curves then represent the hypothetical antenna temperature and optical depth of a 1 km s^{-1}-wide line, or the profile integral of either quantity if $|\tau|$ is small.

Around the curves of N_u/N_l we have placed horizontal error bars displaced by $\pm 1\sigma$ about the mean for the lines of sight toward ζ Per and ζ Oph. Jura & Meyer (1985) found two components with similar conditions toward ζ Per; their results for o Per (not represented here) are similar to those for ζ Oph. For ζ Per, the error bars extend to meet the curve of population ratio and are meant to show the $\pm 1\sigma$ error in T_{exc}. For ζ Oph the case cannot be summarized quite so concisely. The -1σ error bar actually extends indefinitely to the right since the population ratio is bounded above at unity for $T_{exc} > 0$.

---

[2] That is, we may infer comparable excitation from the radio data only if N(CH) is similar in the two directions, as is the case along the narrow optical lines of sight; see also Willson (1981).
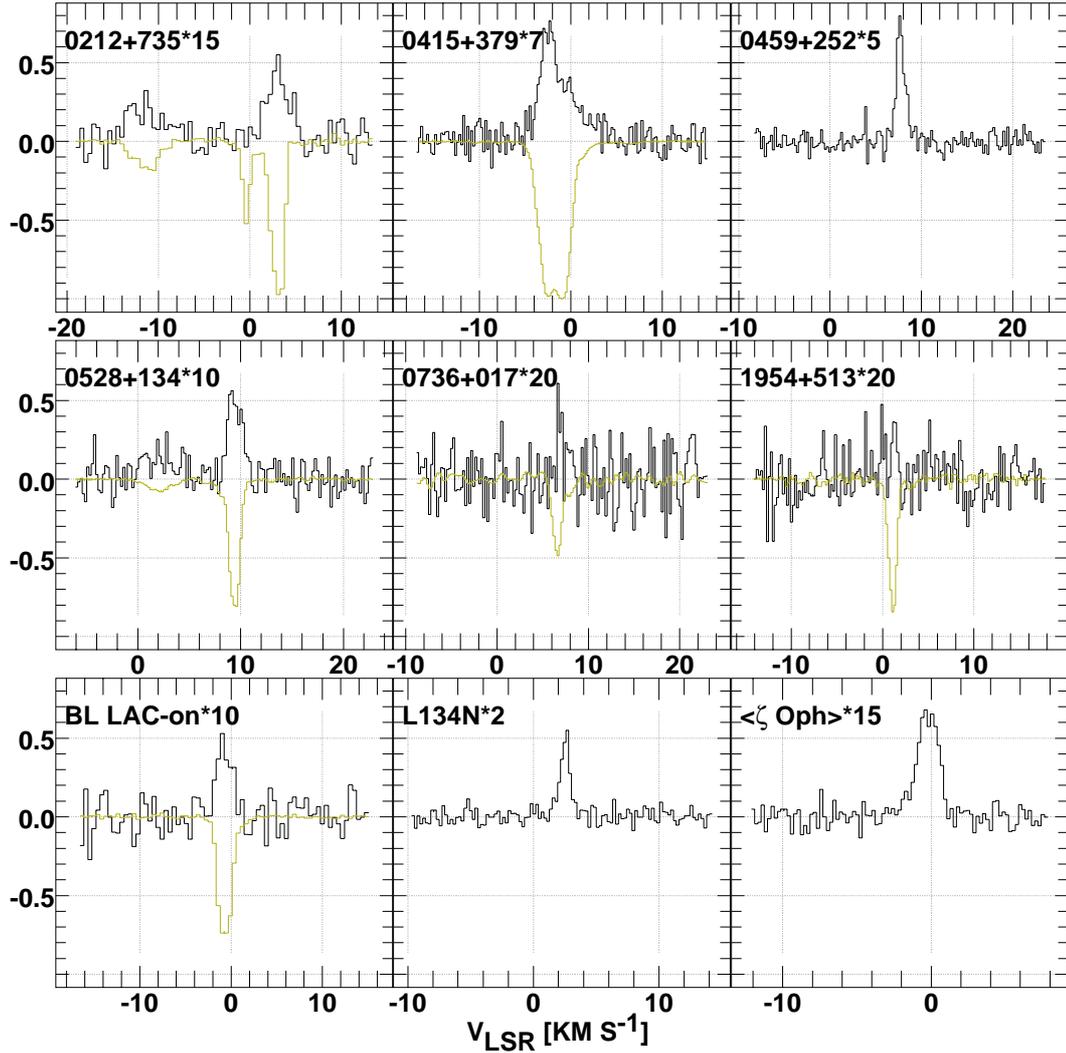
Fig. 4. CH emission profiles (units of Kelvins). For the lines of sight around continuum sources, the profiles are averages of off-source spectra taken 11′ North, East, South and West (except for BL Lac, which is on-source). Shown shaded, where possible, is the corresponding 89 GHz HCO$^+$ $J = 1$–0 absorption profile from Lucas & Liszt (1996) in the form line/continuum-1. At lower right is a spectrum averaged over 80′ in a North-South direction around ζ Oph from Liszt (1997), and a comparison spectrum toward L134N. The emission spectra have been scaled in various ways, as indicated.

Table 2. Background sources observed.

Source	l	b	T_C[1]
B0212+735	128.93°	11.96°	0.79 K
B0224+671	132.12°	6.23 °	0.56 K
B0355+508	150.38°	−1.60°	0.90 K
B0415+379	161.68°	−8.82°	2.79 K
B0433+295	170.58°	−11.66°	7.87 K
B0459+252	177.73°	−9.91°	1.02 K
B0528+134	191.37°	−11.01°	0.75 K
B0727-115	227.77°	3.14°	0.91 K
B0736+017	216.99°	11.38°	0.68 K
B0954+658	145.76°	43.13°	
B1954+513	85.20°	11.90°	0.44 K
B2013+370	74.77°	1.36°	1.95 K
B2023+336	73.03°	−2.23°	0.85 K
B2200+420	92.13°	−10.40°	1.69 K

[1] Gain was approximately 2.5 Jy K^{-1}.

observed are given in Table 2; with the exceptions of 3C123 (B0433+295) and 3C133 (B0459+252) they are all strong mm-wave sources. The observing strategy was like that followed for OH (Liszt & Lucas 1996) and H_2CO (Liszt & Lucas 1995) whereby we observed toward the source and 1.2 HPBW (here, $1.2 \times 9′$) displaced in the four cardinal directions. The beam efficiency of the telescope η_B is usually quoted as 0.7–0.8. We take $\eta_B = 0.7$ because on this scale our profile toward L134N reproduces the canonical value for N_μ(CH) cited in Table 1. We used a channel separation of 2.44 kHz or 0.22 km s^{-1}. The off-source system temperature was typically 38–42 K.

The relationship between brightness of the microwave lines and CH column is nearly always taken in the Rayleigh-Jeans limit for small optical depth because 3335 MHz corresponds to 0.160 K and the excitation temperature is usually taken as either −15 K, following the original observation of Perseus and Orion Arm features toward Cas A (Rydbeck et al. 1976; Hjalmarson et al. 1977) or −60 K (Genzel et al. 1979). These
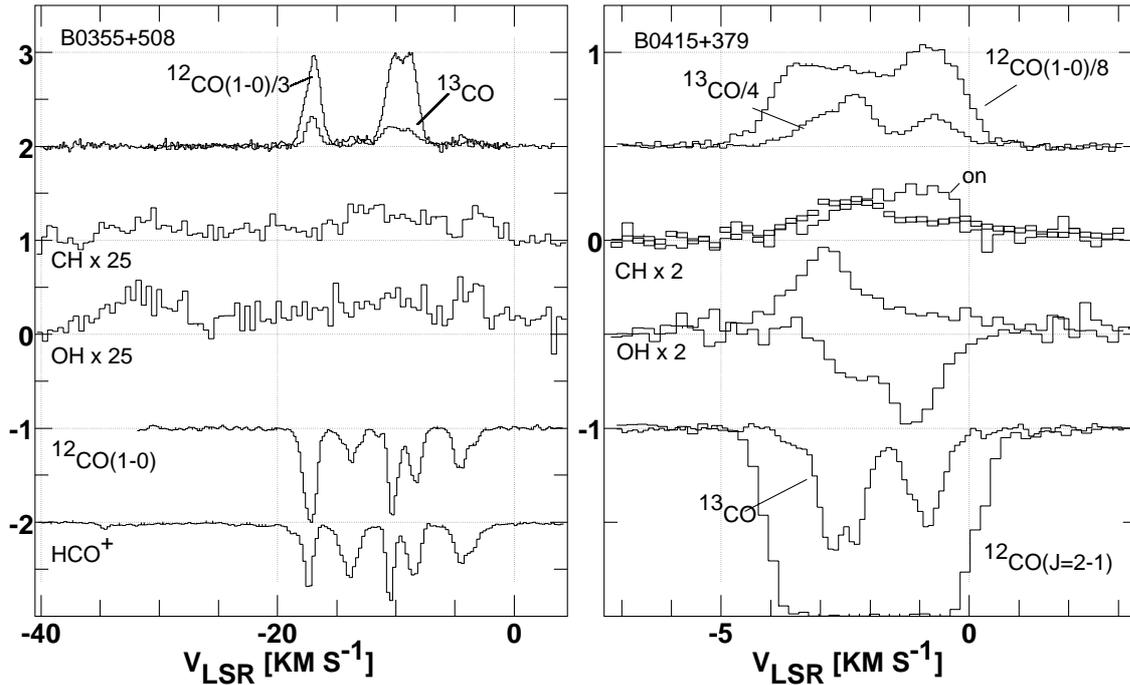
Fig. 5. Spectra of CH and other species toward B0355+508 (left) and B0415+379. For B0415+379 (3C111) both on-source and off-source spectra are shown for CH and OH. The on-source OH spectrum and all the other obvious absorption spectrum are presented in the form (line/continuum-1) while the on-source CH spectra and all the obvious emission spectra are in K. At right, the CO emission spectra at top are for $J = 1–0$ while the absorption spectra at bottom are $J = 2–1$.

values imply that the optical depth is very low, because typical brightnesses are 0.05 K. From atomic physics and thermodynamic equilbrium we have for the $\nu = 3335$ MHz $F' = 1 \rightarrow F'' = 1$ transition the relationship

$$\int \tau_{11} dv = \frac{0.75 N_l \lambda^3 A_{11}(1 - \exp(-h\nu/kT_{exc}))}{8\pi} \quad (1)$$

where $\lambda = c/\nu$, $A_{11} = 2.04 \times 10^{-10}$ s^{-1} and $N_l = N(CH)/(1 + \exp(-h\nu/kT_{exc}))$ is the population in the lower half of the ground-state Λ-doublet, of which a fraction 3/4 is in the $F'' = 1$ level.

This may be used in concert with the relationship between the observed microwave antenna temperature T_A, the excitation temperature T_{exc} and the background continuum temperature against which the line is observed T_{bg}

$$T_A = \eta_B(1 - e^{-\tau})[J(T_{exc}) - J(T_{bg})] \quad (2)$$

where $J(x) \equiv (h\nu/k)/(\exp(h\nu/kx) - 1)$. In the Rayleigh-Jeans limit of small optical depth, with $N(CH)/(1 + \exp(-h\nu/kT_{exc})) \approx N(CH)/2$ one arrives at the relationship

$$N_\mu(CH) = \frac{2.82 \times 10^{14} \text{ cm}^{-2} T_{exc} \int T_A dv}{\eta_B(T_{exc} - T_{bg})}. \quad (3)$$

In the literature, the mantissa of the constant on the right hand side of this expression is sometimes quoted as 2.9, rather than 2.82.

Mean off-source spectra for many lines of sight are shown in Fig. 4 along with HCO$^+$ absorption data (Lucas & Liszt 1996) where possible. Except in two cases (see Sect. 3.4) the on and off-source CH spectra do not differ significantly

and the latter have lower noise levels since they are four-point averages. For BL Lac (B2200+420) we detected CH only toward the source as was also the case in our search for HCO$^+$ *emission*. Also shown are a comparison spectrum toward L134N as well as the mean of the nine spectra observed around ζ Oph and shown individually in Liszt (1997). Line profile integrals and fitted gaussian components are given in the Appendix. CH spectra toward two sources are compared with OH, HCO$^+$ and CO emission and absorption in Fig. 5.

Figure 4 shows that most but not all HCO$^+$ absorption components are seen in CH emission: the HCO$^+$ absorption feature toward B0212+735 which is missing in CH emission is also absent in CO emission, but seen in CO absorption (Liszt & Lucas 1998). The absence of CH absorption hinders our ability to find $N_\mu(CH)$ for components of low column density. Given the vast difference in resolution, the differences in CH and HCO$^+$ profile shapes however interesting, are remarkably slight.

Figure 5 toward B0355+508 shows that CH, like OH, has a diffuse distributed component and does not clearly distinguish individual features in all cases. As discussed by Liszt & Lucas (2000), HCO$^+$ absorption extends out to -36 km s^{-1}, corresponding to the main body of H I absorption in this direction.

Toward 3C111 (B0415+379) the CH is strongly inverted only in the component at higher velocity, which is more chemically complex and likely more nearly fully molecular (see the discussion in Lucas & Liszt 1998). Gas in the lower-velocity component is heavily fractionated in carbon, indicating that only a small fraction of the carbon is in CO. Note that the CO absorption profiles at bottom are for the CO $J = 2–1$ line while the CO emission data shown at top are for $J = 1–0$.
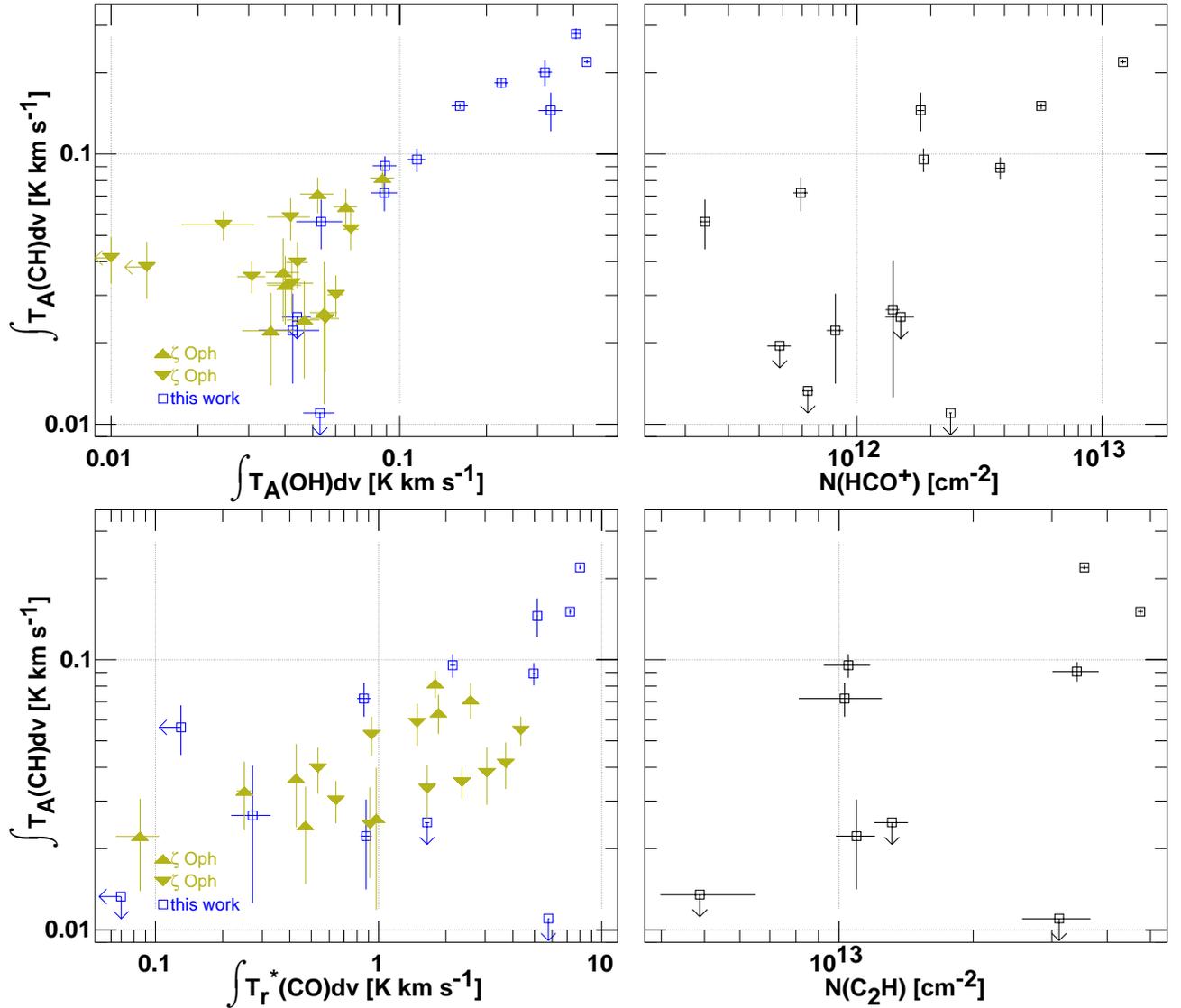
Fig. 6. Comparison of 3335 MHz $F = 1$–1 CH profile integrals with other quantities. Left top: comparison with the OH profile integral toward compact continuum sources (Lucas & Liszt 1996; Liszt & Lucas 1996, 2000) and (heavily shaded) the data of Liszt (1997) around ζ Oph. Left bottom: the CO $J = 1$–0 profile from our 12m telescope data (Liszt & Lucas 1998) and (grayed) the CO data around ζ Oph from Liszt (1997) (see Sect. 2.3). Right top: the HCO^+ column density derived from 89 GHz absorption (Lucas & Liszt 1996). Right bottom: the C_2H column density from mm-wave absorption (Lucas & Liszt 2000a).

For a discussion of CO along this line of sight, see Lucas & Liszt (1998) and Liszt & Lucas (1998).

3.2. CH, OH, HCO$^+$ and C$_2$H

Figure 6 compares the integrated (off-source) CH line strength with several other measures; the quantities used in the figure are given in Table A.1 in the Appendix. The HCO^+ and C_2H absorption (Lucas & Liszt 1996, 2000a) and CO emission (Liszt & Lucas 1998), were taken *on-source* while the OH emission for continuum sources (Liszt & Lucas 1996, 2000) is also off-source data, but displaced further owing to the lower resolution. In this figure we have also included (heavily greyed) our CH, OH and CO data for the diffuse gas around ζ Oph (Liszt 1997). Shown as shaded upward (downward) triangles are the values observed at or to the North (South) of the star;

the profile integrals for positive and negative velocity gas are shown separately because there are actually two components at each position. Around ζ Oph, the observations of CH, OH and CO were concentric. For purposes of nominal comparison $N_\mu(CH) \approx 4 \times 10^{14}$ cm^{-2} $\int T_A dv$ corresponding to $T_{exc} \ll 0$, $\eta_B = 0.7$.

The OH and CH emission profile integrals are tightly correlated for the stronger components. For these features the mean signal-noise weighted ratio of the CH and OH line profile integrals (in the sense CH:OH) is 0.67 ± 0.19. Deriving $N_\mu(CH)$ as given just above and taking the usual formulae for $N_\mu(OH)$ (e.g. Eq. (3) of Liszt & Lucas 1996) with $T_{exc}-T_{cmb} = 1$ or 2 K for OH (*ibid*), we have that $N_\mu(OH)/N_\mu(CH) = 4.3$ or 2.8, in agreement with the result derived optically and quoted in Sect. 2.4, $N(OH)/N(CH) = 3 \pm 0.9$. This serves as a helpful confirmation of the unexpectedly rather small OH main-line excitation

temperatures seen in diffuse gas in the radio and optical (Roueff 1996) regimes. Indirectly, it also suggests that the CH is only weakly inverted ($|T_{exc}|$ is large).

There appear to be two branches of the CH/OH ratio for weak features, one in which the CH brightness increases fairly abruptly at $\int T_A(OH)dv = 0.04-0.05$ K km s^{-1} and another (seen South of ζ Oph) where the CH is relatively strong at small values of the OH integral. The weak CH features showing complicated behaviour in OH and CH are double-valued but well-ordered with respect to a comparison of CH and CO as discussed in Sect. 3.3.

The comparison with both HCO$^+$ and C$_2$H absorption seems to show some sort of bimodality or, at least, a very large range of CH profile integrals at a given $N(HCO^+)$ or $N(C_2H)$. If the fractional abundances of CH and HCO$^+$ are both about constant (which is otherwise believed to be the case for diffuse gas) the 3335 MHz profile integral ($N_\mu(CH)$) does not have a single proportionality to $N(CH)$ for $N(HCO^+) < 3\times10^{12}$ cm^{-2}. Taking the data at face value, for $N(HCO^+) = 10^{12}$ cm^{-2} we have that $N_\mu(CH) \approx 0.8-3 \times 10^{13}$ cm^{-2} or $N(H_2) = 2-8\times10^{20}$ cm^{-2}, leading to $N(HCO^+)/N(H_2) = 1.25-5\times10^{-9}$. The same comparison at $N(HCO^+) = 3 \times 10^{12}$ cm^{-2} and $N_\mu(CH) \approx 5\times10^{13}$ cm^{-2} yields $N(HCO^+)/N(H_2) = 2.5\times10^{-9}$. Earlier, we inferred $N(HCO^+)/N(H_2) = 2-3 \times 10^{-9}$ from the observed tight relationship between HCO$^+$ and OH (Lucas & Liszt 1996; Liszt & Lucas 1996) and we showed that such an unexpectedly high HCO$^+$ abundances suffices to explain the observed quantities of CO for all $N(CO) \lesssim 3\times10^{16}$ cm^{-2} (Liszt & Lucas 2000). A cross-comparison of the $N(CN)/N(H_2)$ ratios determined optically with the column densities of CN and HCO$^+$ seen at mm-wavelengths by Liszt & Lucas (2001) also confirmed this abundance of HCO$^+$.

3.3. CH and CO

For the comparison with CO emission at lower left in Fig. 6, the new data toward continuum sources seemed also to indicate bimodality for the weaker emission. The combined dataset including the points taken around ζ Oph clearly confirms this behaviour for intermediate values of the CO emission profile integral $0.3 \leq W(CO) \leq 5$ K km s^{-1}. The CO emission profile integral is definitely not bimodal with respect to either $N(HCO^+)$ or $N(CO)$ over this range (Liszt & Lucas 1998). A direct comparison between the CO column density measured in absorption and the mm-wave emission brightness shows that $N(CO) \approx 1.25 \times 10^{15}$ cm$^{-2} \int T_r^* dv$ for $\int T_r^* dv = 0.3-4$ K km s^{-1}, see Fig. 12 of Liszt & Lucas (1998).

When the CH brightness is assumed to be proportional to the CH column density, the correlation between CH and H$_2$ then provides for a CO brightness – H$_2$ column density conversion as well. Magnani & Onello (1995) recently compared brightnesses of CH and CO, deriving $N(H_2)$ from $N_\mu(CH)$ by use of the CH–H$_2$ conversion of Mattila (1986) as shown in Fig. 1 and discussed in Sect. 2.1 here. Magnani & Onello (1995) noted a lot of scatter in the CO brightness – H$_2$ column density conversion factors so derived, but did not plot the underlying data, which appear in graphical form here in Fig. 7
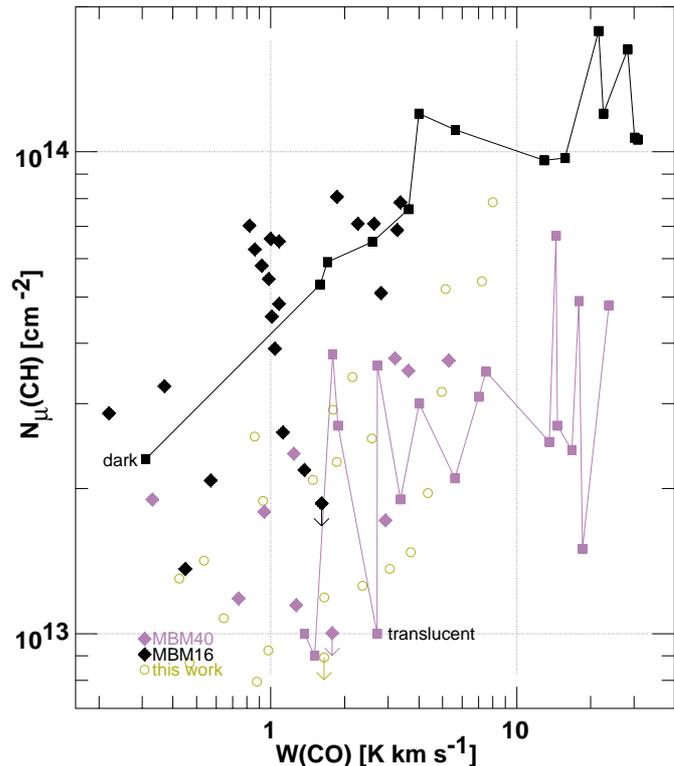

Fig. 7. Microwave-derived CH column densities $N_\mu(CH)$ and CO profile integrals $W(CO)$. The solid, connected symbols represent data tabulated by Magnani & Onello (1995) for lines of sight considered "translucent" (shaded) and "dark" (shown dark). Mapping data for two high-latitude molecular clouds from Magnani et al. (1998) are shown as dark and shaded solid diamonds. Our data from Fig. 6 at bottom left have been overlaid as the open circles.

(nor did they note the bimodal behaviour which is clearly seen there). In passing we note that much of the data for so-called translucent gas was considered to sample diffuse material in the original reference (Federman & Willson 1982).

The chained lines (connected solid symbols) in Fig. 7 show the CH and CO data tabulated by Magnani & Onello (1995), manipulated only to the extent that one source considered translucent (3C353) has been reclassified as dark since an examination of the original reference (Federman et al. 1987) showed that a visual extinction of 6 mag was quoted for the position whose $N_\mu(CH)$ was used. The data from our Fig. 6 at lower left have been transferred to Fig. 7, and it is apparent that they overlap the "translucent" data of Magnani & Onello (1995) except at the very highest values of the CO profile integral. Also shown in Fig. 7 is the more recent mapping data of Magnani et al. (1998) for two high-latitude clouds described as translucent. The observations for one of them, MBM40, all fall into the "translucent" regime; data for MBM 16 lie chiefly on the "dark" gas locus, except at the lowest values of $W(CO)$, and could be interpreted as showing an abrupt transition from diffuse to dark conditions at $W(CO) = 1$ K km s^{-1}.

We can distinguish three modes of behaviour for the data in this figure. First, there is a slow increase of $N_\mu(CH)$ with $W(CO)$ for both the dark and diffuse/translucent gases: possible appearances aside, the best-fit power-law slope for the

"dark" data of Magnani & Onello (1995) has $N_\mu(CH) \propto W(CO)^{0.34\pm0.05}$ while $N_\mu(CH) \propto W(CO)^{0.26\pm0.12}$ for the data along the line marked as "translucent." Second there is a nearly fixed, factor of 3 offset in $N_\mu(CH)$ between the dark cloud and diffuse/translucent material. The CH brightness appears bimodal at a given value of the CO profile integral in a variety of separate datasets and the offset in $N_\mu(CH)$ persists up to CO profile integrals at least as large as 20 K km s^{-1}, which represents quite a strong CO line. For very small CO profile integrals $W(CO) < 1$ K km s^{-1}, the dark and diffuse regimes may merge, which is intuitively understandable. The third discernible mode of behaviour is scatter in $N_\mu(CH)$ at a fixed $W(CO)$ which we ascribed above to variations in CH excitation and other local conditions, for the diffuse/translucent gas.

The strength of CO emission is expected to change rapidly in diffuse gas: $N(H_2) \propto E_{B-V}^2$ from Fig. 1, and $N(CO) \propto N(CH)^2 \propto N(H_2)^2$ (Federman & Lambert 1988; Federman et al. 1994; Liszt & Lucas 2000). So, it follows that the CH profile integral should vary much less rapidly than the CO brightness if $N_\mu(CH) \propto N(CH)$. The change in $N(H_2)$ across Fig. 7 should be smaller than that in $W(CO)$, for the diffuse gas at least, which would lead to a rather shallow slope. But it is far from obvious that the diffuse/translucent and dark gas components should have so nearly the same slope in their $N_\mu(CH)$–$W(CO)$ relationship. Perhaps the shallowness of the slope in the dark gas reflects the decline of X_{CH} in denser gas, at higher $W(CO)$.

A literal interpretation of Fig. 7 implies that dark gas requires about 3 times as much $N(H_2)$ to produce a given $W(CO)$ for $W(CO) = 1$–20 K km s^{-1} (this difference might be larger if $N_\mu(CH)$ is diminished in dark gas because X_{CH} is smaller). If such were the case, a substantial CO emission component from diffuse gas mixed into an ensemble of dark clouds could cause misestimation of $N(H)$. However, there is no other evidence for a diminished $N(H_2)/W(CO)$ ratio in diffuse gas, and actual measurements, in the few possible cases, yield a typical value. For instance, from a comparison of the CO and HCO$^+$ data in Figs. 12 and 13 of Liszt & Lucas (1998), it follows that $N(H_2)/W(CO) \approx 2.5 \times 10^{20}$ H$_2$ cm^{-2}/(K km s^{-1}) around $W(CO) = 1$–2 K km s^{-1}. Toward ζ Oph, where all the relevant properties are directly measureable, we have $N(H_2)/W(CO) \approx 4 \times 10^{20}$ H$_2$ cm^{-2}/(K km s^{-1}) (Liszt 1982, 1997).

3.4. Excitation

Notably, the on-source CH profile is not weaker than the nearby off-source average in a single direction out of all those observed; the CH Λ-doublet is generally inverted in diffuse gas. Figure 8 shows on and off-source spectra taken toward 3C111 and 3C123, the strongest continuum sources observed. Also shown are optical depth spectra made by applying Eq. (2) to the data taken on ($T_{bg} = T_{cmb} + T_C$) and off-source ($T_{bg} = T_{cmb}$). In only one case (3C123) can we derive a statistically significant inversion ($T_{exc} < 0$). Even for 3C111, the excitation temperature derived from a further application of Eq. (2) (using the derived optical depth profile) is positive even where $\tau < 0$ in
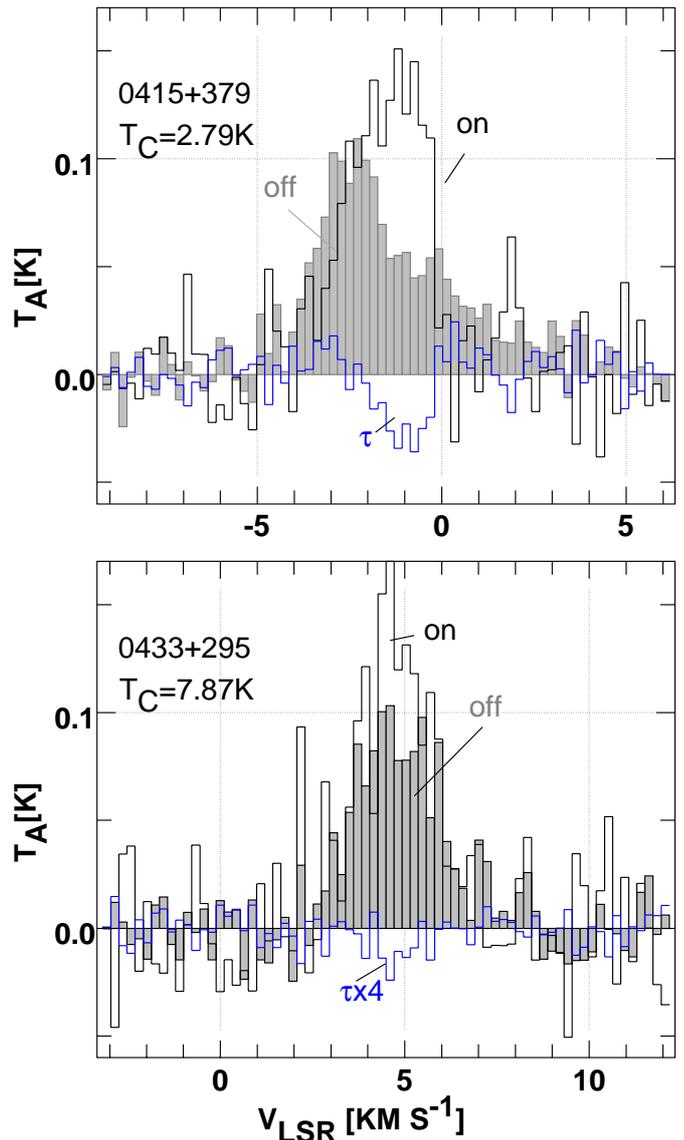

Fig. 8. On and off source spectra toward two strong continuum sources. The off-source average is shown shaded. An optical depth spectrum derived from Eq. (2) is shown in each case; for B0433+295 (3C123) $T_{exc} = -10.7 \pm 3.2$ for the five contiguous central channels showing $\tau < 0$.

Fig. 8; spatial structure in the CH emission renders the solutions unreliable.

For 3C123, however, $\langle T_{exc} \rangle = -10.7 \pm 3.2$ K averaged over the five contiguous central channels where $\tau < 0$ in Fig. 8 and $-16 < T_{exc} < -6$ K over this same interval. This is essentially the same result as that obtained by Hjalmarson et al. (1977), $T_{exc} = -9 \pm 5$ K. Genzel et al. (1979) quote a value $T_{exc} = -60 \pm 30$ K in this direction but the meaning of the (rather large) error or range is not clear from their presentation. Genzel et al. (1979) thus claim that the 3335 MHz transition seen with the 100 m telescope is substantially less inverted than was found earlier using the Onsala 25 m dish. In the optically thin, Rayleigh-Jeans limit of the column density determination $N_\mu(CH) \propto T_{exc}/(T_{exc} - T_{cmb})$. The T_{exc}-dependent term in this expression is 0.96 for $T_{exc} = -60$ K, 0.85 for $T_{exc} = -15$ K, and 0.79 for $T_{exc} = -10$ K.

4. Summary

Although fourth in the current series, this paper is actually also the third of three papers discussing singledish cm-wave spectra of the molecules in diffuse gas, taken toward and around a sample of compact, extragalactic mm-wave continuum sources. In H I, such on-off comparison experiments have come to be known as emission-absorption experiments (Dickey et al. 1978) but as it turns out, we performed one emission-absorption experiment (in OH; Liszt & Lucas 1996), one absorption-absorption experiment (in H_2CO, which appeared in absorption both on and off-source; Liszt & Lucas 1995) and, here, one emission-emission experiment (since no true absorption was detectable).

We began by displaying the richly structured behaviour of CH with E_{B-V}; $N(CH)$ is multi-valued with respect to E_{B-V}, depending on the degree of conversion to molecular gas along the line of sight, and a simple, linear CH–E_{B-V} relationship can be expected only when the extinction is dominated by molecular gas, as toward a single dark cloud. Otherwise, the range of measured $N(CH)$ at a given E_{B-V} in the diffuse gas as a whole is typically more than one order of magnitude. Much of this behaviour can be explained on the basis of an easily-demonstrated and long-known, nearly constant relative abundance $<X_{CH}> = 4.3 \pm 1.9 \times 10^{-8}$, and $N(CH) \propto N(H_2)^{1.00\pm0.06}$ for $N(H_2) \lesssim 10^{21}$ cm^{-2}: as well, we have that $N(H_2) \propto E_{B-V}^{1.8}$ for $0.2 < E_{B-V} < 0.7$.

If CH is a good predictor of H_2, the 140 lines of sight gathered to study the CH–E_{B-V} relationship allow derivation of the molecular fraction in the diffuse/translucent ISM over a much wider range of sample mean densities $<E_{B-V}>/<R>$ than is directly accessible in measurements of the lines of hydrogen. The molecular fraction found in this way is in good agreement with direct measurements at low (Copernicus) and high (FUSE) sample mean density, and is 0.4–0.45 for $<E_{B-V}>/<R> = 0.61$ mag kpc^{-1}, which is the accepted mean in the gas within 500–1000 pc.

We pointed out that sensitive optical measurements of the population ratio in the upper and lower halves of the ground-state CH Λ-doublet toward two stars predict that the brightness of the microwave CH lines should be double-valued at a given CH column density in diffuse gas depending on whether the excitation is inverted (the brighter branch); this is consistent with models of CH excitation which predict a transition from normal excitation to inversion at hydrogen densites in the range 10–1000 cm^{-2}, but the effect is not present in the microwave lines in these directions. This could be due to the disparity in beam-sizes or to relatively small errors in the optical data.

We presented 3335 MHz CH observations toward some of the compact extragalactic mm-wave continuum sources studied in this series of papers, toward two strong cm-wave sources, and around ζ Oph, and compared the properties of CH with those of OH and CO in emission and HCO$^+$ and C_2H seen in absorption. In stronger-lined gas, the CH/OH comparison confirms the very small OH excitation temperatures which have been found in diffuse gas. Comparisons of CH with HCO$^+$ and C_2H show that there is either a very large scatter in the CH brightness or microwave-derived CH column density at a given $N(HCO^+)$ or $N(C_2H)$ or perhaps a bimodality. The CH/HCO$^+$ comparison readily (but only roughly) confirms our previously-derived ratio $N(HCO^+)/N(H_2) = 2 \times 10^{-9}$.

The 3335 MHz line brightness in diffuse gas is very definitely bimodal with regard to CO emission in both the new data presented here and our previously-published data around ζ Oph. To explore this further, we compared our data with other published studies which used CH to derive the CO–H_2 conversion factor in diffuse/translucent gas and found that they are entirely consistent with our data. This may be a manifestation of a disparity between inverted and non-inverted CH expected in diffuse gas.

We found some hitherto-unnoticed systematic behaviour in the CH–CO comparison in diffuse and dark gas, in particular a steady, factor of ≈ 3 offset in the ratio of CH and CO profile integrals for $W(CO) = 1$–30 K km s^{-1}: $W(CH)/W(CO)$ is consistently larger by ≈ 3 in dark gas. A shallow slope in the $W(CH)$–$W(CO)$ relationship in diffuse gas is understandable because the CO abundance varies rapidly with $N(H_2)$, $N(CO) \propto N(H_2)^2$ and the CO brightness will increase even faster than $N(CO)$, but the presence of nearly the same shallow slope $W(CH) \propto W(CO)^{0.3}$ in dark and diffuse gas is puzzling. It may reflect the decline of X_{CH} which is known to occur in very dark gas.

The next paper in this series will discuss several species whose abundances are best determined at cm-wave frequencies, such as NH$_3$, H_2CO and C_4H.

References

Allen, M. M. 1994, ApJ, 424, 754

Bertojo, M., Cheung, A. C., & Townes, C. H. 1976, ApJ, 208, 914

Bohlin, R. C., Savage, B. D., & Drake, J. F. 1978, ApJ, 224, 132

Bouloy, D., Nguyen-Q-Rieu, & Field, D. 1984, A&A, 130, 380

Bujarrabal, V., Salinas, F., & Gonzalo, I. 1984, ApJ, 285, 312

Chaffee, F. H., & Lutz, B. L. 1978, ApJ, 221, L91

Cox, P., Guesten, R., & Henkel, C. 1988, A&A, 206, 108

Crane, P., Lambert, D. L., & Sheffer, Y. 1995, AJS, 99, 107

Crawford, I. A. 1995, MNRAS, 277, 458

Crawford, I. A., & Williams, D. A. 1997, MNRAS, 291, L53

Crutcher, R. M. 1979, ApJ, 234, 881

Crutcher, R. M. 1985, ApJ, 288, 604

Danks, A. C., Federman, S. R., & Lambert, D. L. 1984, A&A, 130, 62

Dickey, J. M., Terzian, Y., & Salpeter, E. E. 1978, AJ Suppl. Ser., 36, 77

Federman, S. R. 1982, ApJ, 257, 125

Federman, S. R., Cardell, J. A., van Dishoeck, E. F., Lambert, D. L., & Black, J. H. 1995, ApJ, 445, 325

Federman, S. R., Evans, N. J., Willson, R. F., et al. 1987, ApJ, 322, 960

Federman, S. R., & Lambert, D. L. 1988, ApJ, 328, 777

Federman, S. R., Strom, C. J., Lambert, D. L., et al. 1994, ApJ, 424, 772

Federman, S. R., & Willson, R. F. 1982, ApJ, 260, 124

Appendix A: Line profile integrals shown in Fig. 6

Table A.1. Line profile integrals.

Source	V	W(OH)	$\int \tau(HCO^+)dv$[1]	$\int \tau(C_2H)dv$[2]	W(CO)	W(CH)
	km s^{-1}	K km s^{-1}	km s^{-1}	km s^{-1}	K km s^{-1}	K km s^{-1}
B0212+735	−10	0.0886(0.009)	0.58(0.04)	0.38(0.18)	0.86(0.06)	0.0719(0.01033)
B0212+735	0	<0.0134	0.62(0.03)	0.18(0.06)	<0.07	<0.01342
B0212+735	3	0.0889(0.0084)	3.77(0.17)	1.26(0.15)	4.96(0.06)	0.0906(0.00748)
B0415+379[3]	−2.2	0.4443(0.0106)	11.91(0.334)	1.31(0.03)	8.00(0.07)	0.2200(0.00389)
B0415+379[4]	−0.8	0.1614(0.0105)	5.526(0.244)	1.75(0.02)	7.22(0.06)	0.1506(0.0037)
B0433+295	all	0.4073(0.0157)				0.2792(0.01294)
B0459+252	all	0.2251(0.0126)				0.1835(0.00838)
B0528+134	2	0.0534(0.0098)	0.2362(0.0103)		<0.13	0.0563(0.01171)
B0528+134	10	0.1146(0.0097)	1.836(0.019)	0.39(0.05)	2.15(0.06)	0.0955(0.00961)
B0727-115	all		0.476(0.052)			<0.0191
B0736+017	all	0.0426(0.0101)	0.802(0.063)	0.40(0.04)	0.88(0.05)	0.0223(0.00813)
B0954+658	all	0.0442(0.0050)	1.48(0.20)	0.48(0.04)	1.65(0.04)	<0.025
B2013+370	all	0.3332(0.0310)	1.785(0.0236)		5.15(0.23)	0.1452(0.02359)
B2023+336	all	0.3185(0.0173)				0.2009(0.0219)
B2200+420	all	0.0529(0.0066)	2.36(0.03)	1.15(0.20)	5.78(0.05)	<0.011

[1] $N(HCO^+) = 1.02 \times 10^{12}$ cm^{-2} $\int \tau(HCO^+)dv$.
[2] $N(C_2H) = 2.711 \times 10^{13}$ cm^{-2} $\int \tau(C_2H)dv$.
[3] HCO$^+$ data toward B0415+379 are $60 \times N(H^{13}CO^+)$.
[4] Toward 3C111 components were separated by Gaussian fitting.

Felenbok, P., & Roueff, E. 1996, ApJ, 465, L57
Genzel, R., Downes, D., Pauls, T., Wilson, T. L., & Bieging, J. 1979, A&A, 73, 253
Glassgold, A. E., & Langer, W. D. 1975, ApJ, 197, 347
Glassgold, A. E., & Langer, W. D. 1976, ApJ, 206, 85
Gredel, R., van Dishoeck, E. F., & Black, J. H. 1993, A&A, 269, 477
Hjalmarson, A., Sume, A., Elldér, J., et al. 1977, AJS, 35, 263
Jenniskens, P., Ehrenfreund, P., & Desert, F.-X. 1992, A&A, 265, L1
Joseph, C. L., Snow, T. P., Seab, C. G., & Crutcher, R. M. 1986, ApJ, 309, 771
Jura, M., & Meyer, D. M. 1985, ApJ, 294, 238
Lang, K. R., & Willson, R. F. 1978, ApJ, 224, 125
Lien, D. J. 1984, ApJ, 284, 578
Liszt, H. S. 1982, ApJ, 262, 198
Liszt, H. S. 1997, A&A, 322, 962
Liszt, H. S., & Lucas, R. 1995, A&A, 299, 847
Liszt, H. S., & Lucas, R. 1996, A&A, 314, 917
Liszt, H. S., & Lucas, R. 1998, A&A, 339, 561
Liszt, H. S., & Lucas, R. 2000, A&A, 355, 333
Liszt, H., & Lucas, R. 2001, A&A, 370, 576
Lucas, R., & Liszt, H. S. 1998, A&A, 337, 246
Lucas, R., & Liszt, H. S. 1996, A&A, 307, 237
Lucas, R., & Liszt, H. S. 2000a, A&A, 358, 1069
Lucas, R., & Liszt, H. S. 2000b, A&A, 355, 327
Lucas, R., & Liszt, H. S. 2002, A&A, 384, 1054
Münch, I. G. 1952, ApJ, 116, 575
Magnani, L., & Onello, J. S. 1995, ApJ, 443, 169
Magnani, L., Onello, J. S., Adams, N. G., Hartmann, D., & Thaddeus, P. 1998, ApJ, 504, 290

Mattila, K. 1986, A&A, 160, 157
Meyer, D. M., & Roth, K. C. 1991, ApJ, 376, L49
Nash, A. G. 1990, AJS, 72, 303
Ohishi, M., Irvine, W., & Kaifu, N. 1992, in Astrochemistry of cosmic phenomena: proceedings of the 150th Symposium of the International Astronomical Union, held at Campos do Jordao, Sao Paulo, Brazil, August 5–9, 1991, ed. P. D. Singh (Dordrecht: Kluwer 1992), 171
Penprase, B. E. 1993, AJS, 88, 433
Rachford, B., Snow, T. P., Tumlinson, J., et al. 2002, ApJ, in press
Rachford, B. L., Snow, T. P., Tumlinson, J., et al. 2001, ApJ, 555, 839
Roueff, E. 1996, MNRAS, 279, L37
Rydbeck, O. E. H., Kollberg, E., Hjalmarson, A., et al. 1976, AJS, 31, 333
Sandell, G. 1982, in Regions of Recent Star Formation, ed. R. S. Roger, & P. E. Dewdney, ASSL, 93, 479
Sandell, G., Johansson, L. E. B., Rieu, N. Q., & Mattila, K. 1981, A&A, 97, 317
Savage, B. D., Drake, J. F., Budich, W., & Bohlin, R. C. 1977, ApJ, 216, 291
Snow, T. P., Rachford, B. L., Tumlinson, J., et al. 2000, ApJ, 538, L65
Spitzer, L. 1978, Physical processes in the interstellar medium (New York Wiley-Interscience), 333
Van Dishoeck, E. F., & Black, J. H. 1986, AJS, 62, 109
van Dishoeck, E. F., & Black, J. H. 1989, ApJ, 340, 273
Willson, R. F. 1981, ApJ, 247, 116